

Deconstructing symmetry breaking dynamics

Fumika Suzuki^{1,2,*} and Wojciech H. Zurek¹

¹*Theoretical Division, Los Alamos National Laboratory, Los Alamos, New Mexico 87545, USA*

²*Center for Nonlinear Studies, Los Alamos National Laboratory, Los Alamos, New Mexico 87545, USA*

(Dated: December 1, 2025)

The Kibble-Zurek mechanism (KZM) successfully predicts the density of topological defects deposited by the phase transitions, but it is not clear why. Its key conjecture is that, near the critical point of the second-order phase transition, critical slowing down will result in a period when the system is too sluggish to follow the potential that is changing faster than its reaction time. The correlation length at the freeze-out instant \hat{t} when the order parameter catches up with the post-transition broken symmetry configuration is then decisive, determining when the mosaic of broken symmetry domains locks in topological defects. To understand why the KZM works so well we analyze Landau-Ginzburg model and show why temporal evolution of the order parameter plays such a key role. The analytical solutions we obtain suggest novel, hitherto unexplored, experimentally accessible observables that can shed light on symmetry breaking dynamics while testing the conjecture on which the KZM is based.

The Kibble-Zurek mechanism (KZM) combines Kibble's insight [1, 2] that, during cosmological phase transitions, the causal independence of distinct Hubble volumes leads to independent choices of broken symmetry and thus to the formation of topological defects, with the realization [3–5] that the universality class and associated critical exponents determine how the defect density scales with the quench rate in a second-order phase transition. This scaling is based on a conjecture about the dynamics of the order parameter near the critical point: It uses equilibrium properties of the transition, such as the critical scaling of the relaxation time and the healing length, to predict a nonequilibrium outcome — the relic density of topological defects formed after the transition. The “freeze-out” (or “adiabatic-impulse-adiabatic” approximation) and the “sonic horizon” paradigms explain the defect density by focusing on different aspects of the order parameter dynamics in the near-critical region. Despite their differences, both approaches lead to the same scaling law. We deconstruct the order parameter dynamics in the Landau-Ginzburg model of the phase transition to identify the origin of the KZM scaling.

Critical slowing down plays the key role. The relaxation time diverges in the vicinity of the critical point with vanishing ϵ , the dimensionless distance from the critical point:

$$\tau(\epsilon(t)) \cong \tau_o / |\epsilon(t)|^{\nu z}.$$

Above, ν and z are critical exponents. The freeze-out paradigm compares it with the timescale $\epsilon/\dot{\epsilon}$ on which the distance from the critical point varies during the quench that can be induced, e.g., by the change of pressure or temperature. In the narrow near-critical range linear dependence on time:

$$\epsilon(t) = t/\tau_Q$$

with τ_Q the quench timescale can be usually assumed. Hence;

$$\epsilon/\dot{\epsilon} = t.$$

Consequently, relaxation time $\tau(\epsilon)$ and $\epsilon/\dot{\epsilon}$ (i.e., time from the critical point) equal at the instant $t = \pm \hat{t}$ when $\tau_o/|\hat{t}/\tau_Q|^{\nu z} = \hat{t}$. Thus:

$$\hat{t} = (\tau_o \tau_Q^{\nu z})^{\frac{1}{1+\nu z}},$$

and;

$$\hat{\epsilon} = \hat{t}/\tau_Q = \left(\frac{\tau_o}{\tau_Q}\right)^{\frac{1}{1+\nu z}}.$$

The KZM asserts that the evolution of the order parameter will cease to be adiabatic at $t \approx -\hat{t}$ before the critical point, enter an impulse regime where the changes imposed by the quench outpace relaxation, and will return to adiabatic after $t = +\hat{t}$, but with the initial conditions set by the fluctuations introduced before $+\hat{t}$.

To estimate defect density one recognizes [3–5] that at the freezeout time \hat{t} the correlation length is:

$$\hat{\xi} = \xi_o / |\hat{\epsilon}|^{\nu} = \xi_o \left(\frac{\tau_Q}{\tau_o}\right)^{\frac{\nu}{1+\nu z}}.$$

A single “unit” of topological defect (e.g., a single monopole, a section of the line defect, or a “tile” of a domain wall) is then expected to appear in a domain of size $\hat{\xi}$. This leads to the estimated dependence of the defect density on the quench time τ_Q :

$$\mathcal{N} \simeq \hat{\xi}^d / \hat{\xi}^D = \xi_o^{(d-D)} \left(\frac{\tau_Q}{\tau_o}\right)^{(d-D) \frac{\nu}{1+\nu z}}.$$

Above, d is the dimensionality of defects ($d = 0$ for monopoles, $d = 1$ for string-like flux lines, and $d = 2$ for domain walls), and $D > d$ is the dimensionality of the space, while ξ_o and τ_o are determined by microphysics.

* fsuzuki@lanl.gov

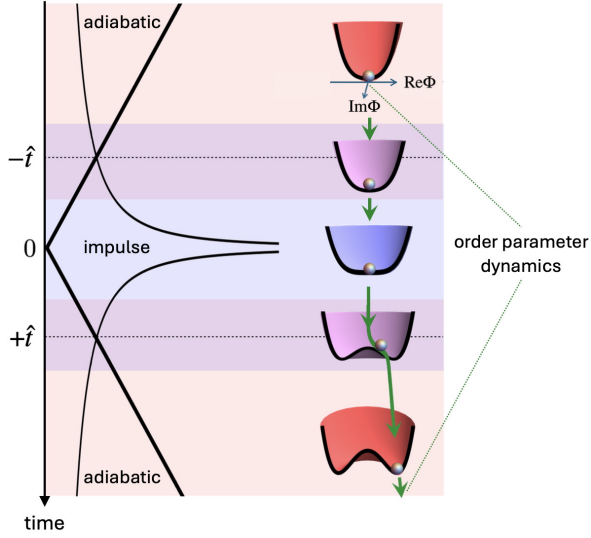


FIG. 1: Symmetry breaking dynamics in a second order phase transition. Landau-Ginzburg model attributes symmetry breaking to the change of the thermodynamic potential from the single-minimum parabola (top) to the degenerate minima (bottom). When the order parameter is a real field (case represented by the dark line above) there are just two broken symmetry minima. When the field is complex (i.e., order parameter in a superfluid), the potential assumes a “sombbrero” shape, with continuum of the broken symmetry states. We investigate how the temporal evolution of the order parameter (which starts for $t < 0$ in the single symmetric minimum, but must choose one of the broken symmetry possibilities after the transition, see Fig. 3) leads to the mosaic of domains that lock in topological defects. The Kibble-Zurek mechanism posits that the size of these domains is set by the correlation length at the instant $+t$ when the order parameter catches up with the new broken symmetry minimum. We show that this temporal evolution can be analyzed using ordinary differential equations with solutions that mark the freeze-out instant $+t$.

The sonic horizon paradigm focuses instead on the growth of broken symmetry domains from the preexisting fluctuations that act as seeds. The relevant sound velocity with which the newly selected broken symmetry vacuum spreads is expected to be:

$$u = \xi(\epsilon)/\tau(\epsilon) = (\xi_o/\tau_o)|\epsilon|^{\nu(z-1)}.$$

When the front of the new broken symmetry phase propagates with this velocity over the time interval $\sim t$, the size of the domains that choose the same broken symmetry scales as $\hat{\xi} = \xi_o(\frac{\tau_Q}{\tau_o})^{\frac{\nu}{1+\nu z}}$, as in the freeze-out paradigm. The defect density \mathcal{N} derived above also follows.

Both paradigms are discussed in [3–6], where it is emphasized that the crucial prediction of the KZM is the scaling of the post-transition defect density with the

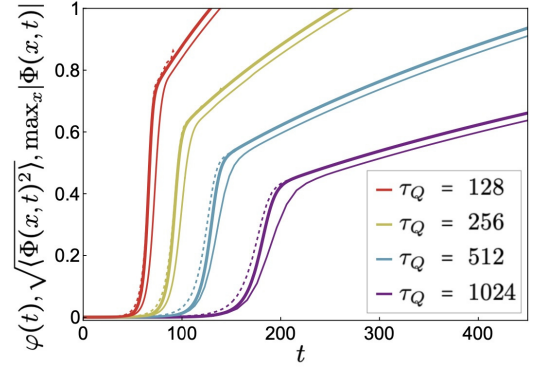


FIG. 2: Time evolution of the order parameter: comparison between the analytical solution of the ordinary differential equation (2) and the numerical solution of the Langevin equation for a real scalar field in (1+1) dimensions [1]. The thick lines represent the analytical solutions $\varphi(t)$ (Eq. (4)) with $\eta = 1$ and $\varphi(0) = 10^{-4}$ for various quench timescales τ_Q , while the numerical results $\sqrt{\langle \Phi(x, t)^2 \rangle}$ (thin lines), $\max_x |\Phi(x, t)|$ (dashed lines) are obtained by solving Eq. (1) with $\eta = 1$ and $\theta = 10^{-8}$. From left to right, $\tau_Q = 128, 256, 512, 1024$ respectively.

quench time. Although the physical pictures invoked by the two paradigms differ, they can nevertheless peacefully coexist in both quantum and classical settings [7]. This coexistence, and especially the fact that they yield essentially the same scaling, is surprising, as there are transitions that rely on different, non-sonic modes of propagation of the broken symmetry phase front. For instance, transitions involving conserved order parameter [8, 9] or diffusive spreading of the new phase [10, 11] do not fit the sonic horizon scenario, and neither does structure formation in steady state (rather than equilibrium) settings [12, 13] such as Rayleigh-Benard instability. There even exists an example [14] where spatial degrees of freedom are absent.

We conclude that the temporal evolution encapsulated in the freeze-out paradigm captures the essential dynamics of phase transitions relevant for defect formation. Our aim is to understand why this is the case. We will show that the temporal evolution of the order parameter plays a central role and captures the essence of the KZM. Moreover, our results highlight a new observable that has so far remained largely unexplored but should be accessible experimentally: the quench-induced temporal evolution of the order parameter in the near-critical region (Fig. 1).

DECONSTRUCTING THE KIBBLE-ZUREK MECHANISM: THE TEMPORAL EVOLUTION

The usual “workhorse” in the study of the nonequilibrium dynamics during symmetry-breaking phase transi-

tions is a Langevin partial differential equation (PDE) with a time-dependent Landau-Ginzburg potential, $V(\Phi) = (\Phi^4 - 2\epsilon(t)\Phi^2)/8$, for the real scalar field Φ representing the order parameter [15–20]:

$$\ddot{\Phi}(\mathbf{x}, t) + \eta \dot{\Phi}(\mathbf{x}, t) - \nabla^2 \Phi(\mathbf{x}, t) + \partial_{\Phi} V(\Phi) = \vartheta(\mathbf{x}, t) \quad (1)$$

where the noise term ϑ has correlations given by;

$$\langle \vartheta(\mathbf{x}, t), \vartheta(\mathbf{x}', t') \rangle = 2\eta\theta\delta(\mathbf{x}' - \mathbf{x})\delta(t' - t).$$

Here, η represents the damping constant, and θ is the temperature of the reservoir.

We now “deconstruct” the Langevin PDE used to study defect formation, and consider temporal evolution separately from its spatial part and the noise. As we shall see, the resulting dynamics of the order parameter suggests the succession of the adiabatic-impulse-adiabatic stages. Distinguishing between these stages helps explain why the instants $-\hat{t}$ and $+\hat{t}$, which mark the transitions between them, are crucial for establishing the KZM scaling.

We focus on the ordinary differential equation (ODE) in which $\varphi(t)$ depends solely on time:

$$\ddot{\varphi}(t) + \eta \dot{\varphi}(t) = -\partial_{\varphi} V(\varphi(t)) \quad (2)$$

obtained from Eq. (1) by omitting the spatial degrees of freedom and the noise term. It captures the essence of the temporal behavior of the order parameter $\varphi(t)$ without the need to rely on the full PDE (Eq. (1)). Indeed, in the overdamped case where $\ddot{\varphi}(t) \ll \eta \dot{\varphi}(t)$, Eq. (2) is a Bernoulli ODE,

$$\eta \dot{\varphi}(t) + \frac{1}{2}(\varphi(t)^3 - \epsilon(t)\varphi(t)) = 0 \quad (3)$$

which can be solved analytically:

$$\frac{\varphi(t)}{\varphi(0)} = \frac{e^{t^2/4\eta\tau_Q}}{\sqrt{1 + \varphi(0)^2 \sqrt{\frac{\pi\tau_Q}{2\eta}} \operatorname{erfi}\left(\frac{t}{\sqrt{2\eta\tau_Q}}\right)}} \quad (4)$$

where $\varphi(0) = \varphi(t=0)$ and $\operatorname{erfi}(y) = \frac{2}{\sqrt{\pi}} \int_0^y e^{y'^2} dy'$. This function predicts the evolution of the order parameter in symmetry-breaking phase transitions that can be modeled by Landau-Ginzburg theory. Indeed, the time evolution of the order parameter given by numerical simulation of the Langevin PDE, Eq. (1) in (1+1) dimensions, is in close agreement with the analytical solution of $\varphi(t)$ as shown in Fig. 2. Thus, $\sqrt{\langle \Phi(x, t)^2 \rangle}$ (thin lines) obtained by averaging over the spatial dependence of $\Phi(x, t)^2$ is somewhat smaller than the solution of Bernoulli ODE given by Eq. (4) (thick lines), as its value is suppressed by the presence of topological defects. Maximum values of $|\Phi(x, t)|$, $\max_x |\Phi(x, t)|$ (dashed lines), by contrast, are slightly larger than $\varphi(t)$, enhanced by the random walk due to noise. Therefore, the evolution of the order parameter φ is largely captured by solving the ODE Eq.

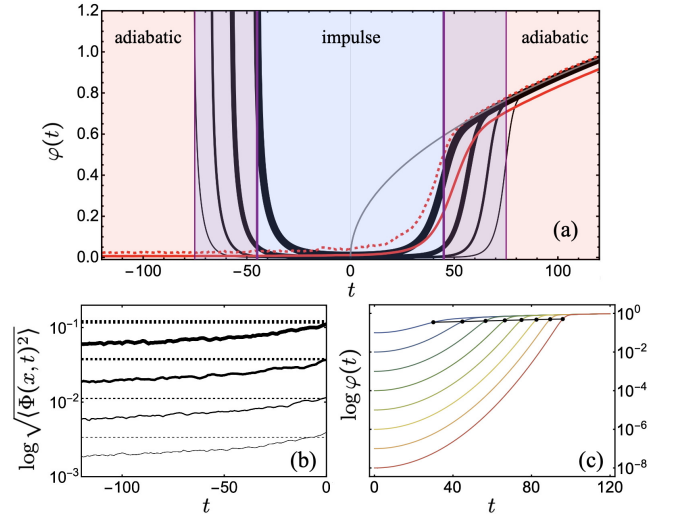


FIG. 3: Order parameter dynamics for varying noise temperature θ and initial conditions $\varphi(0)$. (a) The order parameter $\varphi(t)$ from Eq. (4) for $\eta = 1$, $\tau_Q = 128$, and $\varphi(0) = 10^{-2}, 10^{-3}, 10^{-4}, 10^{-5}$ (thick to thin lines), compared with numerical results: $\sqrt{\langle \Phi^2 \rangle}$ (solid red) and $\max_x |\Phi|$ (dashed red) from Eq. (1) for a real scalar field in (1+1) dimensions with $\eta = 1$, $\theta = 10^{-4}$ (see Fig. 2). The gray line shows equilibrium $|\varphi_{\min}| = \sqrt{\epsilon}$. Vertical purple lines mark $\pm \hat{t}$ for $\varphi(0) = 10^{-2}$ (thick) and 10^{-5} (thin). (b) Noise-induced $\sqrt{\langle \Phi^2 \rangle}$ with $\theta = 10^{-2}$ to 10^{-5} (thick to thin) slowly accumulates before $t = 0$, setting $\varphi(0) \approx \sqrt{\langle \Phi(x, t=0)^2 \rangle} \approx \frac{1}{2} \sqrt{2\theta/\epsilon}$ (dashed lines) for rapid post-transition growth. (c) Plots of $\log \varphi(t)$ for $\varphi(0) = 10^{-1} \dots 10^{-8}$. As $\varphi(t) \approx \varphi(0) e^{t^2/4\eta\tau_Q}$ when $t \in [-\hat{t}, +\hat{t}]$, order parameter buffeted by noise is amplified, but the freeze-out time $+\hat{t}$ depends only logarithmically on $\varphi(0)$, making it insensitive to its precise value, and, hence, insensitive to θ , the noise temperature.

(2). As that temporal equation is the same in multi-dimensional spaces, we expect that our conclusions also follow when there is more than one spatial dimension.

In the pre-transition symmetric phase, noise leads to fluctuations around $\varphi = 0$, as shown in Fig. 3. This behavior is, of course, not observed when solutions of the noise-free Eq. (2) are traced back to the pre-freezeout epoch, $t \leq -\hat{t}$, since—consistent with the Bernoulli equation—the order parameter can attain a finite and modest value at $t = 0$ only if it starts with a suitably large $|\varphi(t)|$ in the distant pre-transition past (Fig 3 (a)). By contrast, in numerical solutions of the Langevin PDE, the accumulation of noise results in a modestly fluctuating $\varphi(t)$ in the near-critical regime. The influence of the noise is thus effectively encoded in the “initial condition” $\varphi(0)$, and the resulting dependence of $\varphi(0)$ on θ can be estimated: Before $t = 0$, the potential is a harmonic $V_{\text{har}}(\Phi) = -\frac{1}{4}\epsilon(t)\Phi^2$ near $\Phi = 0$. Since the temperature θ corresponds to the kinetic energy of Φ , we can estimate

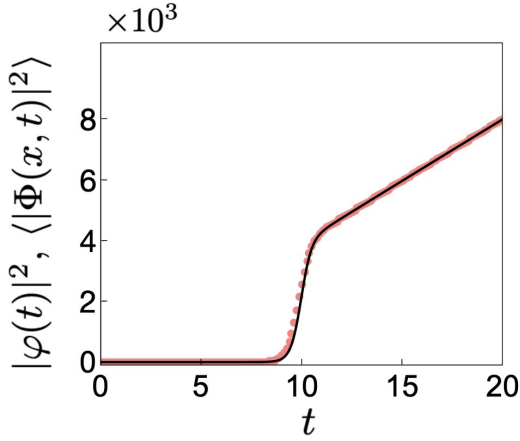


FIG. 4: Order parameter evolution for the Gross–Pitaevskii equation. The black line represents the analytical solution for the condensate number density $|\varphi(t)|^2$ (Eq. (8)) with $\varphi(0) = 3 \times 10^{-3}$, while the corresponding numerical result $\langle |\Phi(x, t)|^2 \rangle$ (light red dots) is obtained by solving the stochastic Gross–Pitaevskii equation Eq. (5) in (1+1) dimensions for a complex wave function-like order parameter with $\theta = 10^{-3}$. For both plots, $\gamma = 10^{-2}$, $g = 0.05$, and quench timescale $\tau_Q = 0.05$.

$\sqrt{\langle \Phi^2 \rangle} \approx \frac{1}{2} \sqrt{2\theta/(-\epsilon(t))}$ where the factor 1/2 results from averaging over x (Fig. 3 (b)). More precise estimate is not really needed for our purpose, as the all-important \hat{t} depends only logarithmically on $\varphi(0)$ (and, hence, on $\sqrt{\langle \Phi(x, t=0)^2 \rangle}$) (Fig. 3 (c)).

EVOLUTION OF THE GROSS-PITAEVSKII WAVE FUNCTION

This approach also applies to a complex wave function-like order parameter $\Phi(\mathbf{x}, t)$, such as in the stochastic Gross–Pitaevskii equation, which is commonly used to describe Bose–Einstein condensates [21–26] and can be written as

$$(i - \gamma)\dot{\Phi}(\mathbf{x}, t) = -\frac{1}{2}\nabla^2\Phi(\mathbf{x}, t) - \epsilon(t)\Phi(\mathbf{x}, t) + g|\Phi(\mathbf{x}, t)|^2\Phi(\mathbf{x}, t) + \vartheta(\mathbf{x}, t) \quad (5)$$

where γ represents the dissipation and g is the non-linearity parameter.

In this case as well, the equation can be deconstructed into a temporal ODE by omitting the spatial degrees of freedom and the noise term:

$$(i - \gamma)\dot{\varphi}(t) = -\epsilon(t)\varphi(t) + g|\varphi(t)|^2\varphi(t). \quad (6)$$

Applying the ansatz $\varphi = |\varphi(t)|e^{i\Theta(t)}$ to the condensate wavefunction, this equation also yields an analytically solvable form of the Bernoulli ODE for $|\varphi(t)|$:

$$(1 + \gamma^2)\frac{d|\varphi(t)|}{dt} = \gamma\epsilon(t)|\varphi(t)| - \gamma g|\varphi(t)|^3. \quad (7)$$

Its solution can be written as

$$\frac{|\varphi(t)|}{|\varphi(0)|} = \frac{e^{\gamma t^2/2(1+\gamma^2)\tau_Q}}{\sqrt{1 + g\varphi(0)^2 \sqrt{\frac{\pi\gamma\tau_Q}{1+\gamma^2}} \operatorname{erfi}\left(\frac{\sqrt{\gamma}t}{\sqrt{(1+\gamma^2)\tau_Q}}\right)}} \quad (8)$$

where $\varphi(0)$ is determined by the size of the noise.

Fig. 4 shows a comparison between the numerical solution of the stochastic Gross–Pitaevskii equation (Eq. (5)), representing the time evolution of the condensate number density $\langle |\Phi(x, t)|^2 \rangle$ (spatially averaged), and that given by the analytical solution (Eq. (8))¹.

This result demonstrates that analytical functions as simple as Eqs. (4, 8) can capture surprisingly well the time evolution of the order parameter in symmetry-breaking phase transitions for broad range of systems that can be modeled within the Langevin / Landau-Ginzburg or Gross-Pitaevskii framework. The experimentally accessible time evolution of the order parameter in transitions involving magnetization, polarization or condensate density could be modeled using Eqs. (4, 8).

The KZM does not directly address the time evolution of the order parameter. Nevertheless, the temporal behavior of the order parameter we discussed anticipates its essential features. In the next section, we show how these features emerge and relate them to the core concepts of the mechanism.

EVOLUTION OF THE ORDER PARAMETER AND THE KIBBLE-ZUREK MECHANISM

The key insight [3–5] that leads to the KZM scaling is the realization that, near the critical point of the second-order phase transition, critical slowing down will result in a time interval $[-\hat{t}, +\hat{t}]$ where the order parameter is too sluggish to adjust to the potential which is changing faster than its reaction time. Thus, while outside this interval the order parameter can be in approximate equilibrium, within the interval $[-\hat{t}, +\hat{t}]$ its evolution “cannot keep up” with time-dependent $V(\Phi)$. This is of little consequence when $t < 0$, as prior to symmetry breaking the order parameter only fluctuates around the symmetric vacuum. Nevertheless, fluctuations imparted near and especially after $-\hat{t}$ are unconstrained by $V(\Phi)$. They seed topological defects that germinate as $\Phi(x, t)$ begins to catch up when $t > 0$ with the local broken symmetry minima of the potential. As a consequence, near $+\hat{t}$ defects become frozen in the broken symmetry configuration in ways that depend on the nature of the system [7].

¹ We note that in the simulations of the Gross-Pitaevskii equation “truncated Wigner method” (see, e.g., [27]) is often employed, with the noise introduced to the initial $\Phi(x, t)$. Thus, unlike in the case of the Langevin Eq. (1) (where noise is injected while the system evolves), quantum fluctuations at or before at $-\hat{t}$ would evolve into the seeds of topological defects at $+\hat{t}$.

The KZM scaling appears to be insensitive to the details of that evolution.

This broad applicability of the KZM suggests that, as proposed in [3–5], the critical slowing down is key to its success. We now return to Fig. 3 to discuss the connection between the KZM and the dynamics of the order parameter. Fig. 3 (a) shows the plot of the solution (Eq. (4)) with $\eta = 1$, $\tau_Q = 128$ for several values of $\varphi(0)$. After $t = 0$ all exhibit similar behavior: The initial period (where $\varphi(t)$ slowly increases till $+\hat{t}$) is followed by a “jump” where the solution catches up with the local broken symmetry equilibrium, and thereafter follows the broken symmetry minimum of the Landau-Ginzburg potential.

This behavior is suggested by the adiabatic-impulse-adiabatic scenario [3–6], and was seen in numerical simulations [28, 29]. The start of the rapid rise can be identified with the freeze-out time $+\hat{t}$, when the order parameter evolution switches from the sluggish pre-transition pace to catch up with the post-transition broken symmetry equilibrium value $\sim \sqrt{\epsilon(t)}$. Note that before $t = 0$ (when the critical point is transversed) solution $\varphi(t)$ of Eq. (2) “jumps down” to relatively small values in the impulse regime, reaching them at the instant suggestive of $-\hat{t}$. When $t \in [-\hat{t}, +\hat{t}]$ evolution is slow compared to these two “jumps”. As was already discussed, noise plays a key role there.

Fig. 3 (c) shows the plots of $\log(\varphi)$ for various $\varphi(0)$. Black circles indicate the freeze-out time $+\hat{t}$ for each $\varphi(0)$, where $\dot{\varphi} = 0$. This inflection point signifies a “jump” which we identify with $+\hat{t}$. It demonstrates that the instants $\pm\hat{t}$ depend only logarithmically on $\varphi(0)$ at the critical point that incorporates the effect of the noise.

Plotting the rescaled solution $\tilde{\varphi}(\tilde{t})$, where $\tilde{\varphi} = \sqrt[4]{\tau_Q/\eta}\varphi$ and $\tilde{t} = t/\sqrt{\eta\tau_Q}$, reveals a clear similarity among the curves for different quench timescales τ_Q in the overdamped regime (Fig. 5(a)), along with only a slow (logarithmic) dependence on the initial value of the order parameter $\varphi(0)$ (hence, only logarithmic dependence on the temperature of the noise).

It follows that, in accord with Eq. (4), the freeze-out time \hat{t} obeys the relationship [3–5, 16]

$$\hat{t} \propto \sqrt{\eta\tau_Q} \quad (9)$$

in the overdamped case.

UNDERDAMPED AND OVERDAMPED EVOLUTION

For the underdamped case, Eq. (2) can be solved numerically. Fig. 5 (b) depicts the rescaled solution $\tilde{\varphi}(\tilde{t})$ of Eq. (2) where the second term $\eta\dot{\varphi}$ is neglected and $\tilde{\varphi} = \tau_Q^{1/3}\varphi$, $\tilde{t} = t/\tau_Q^{1/3}$. After this rescaling, the solutions corresponding to different quench timescales τ_Q exhibit a clear similarity.

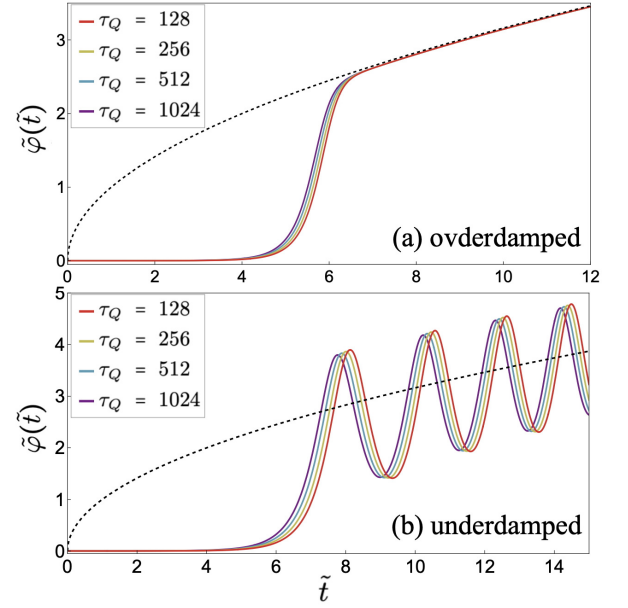


FIG. 5: Order parameter dynamics given by Eq. (2) in the overdamped and underdamped cases corresponding to a real scalar field described by the Langevin equation. The rescaled solution $\tilde{\varphi}(\tilde{t})$ in the overdamped case with $\eta = 1$ where the first term $\dot{\varphi}$ of Eq. (2) is discarded (a) and in the underdamped case where the second term $\eta\dot{\varphi}$ of Eq. (2) is discarded (b). $\tilde{\varphi} = \sqrt[4]{\tau_Q/\eta}\varphi$ and $\tilde{t} = t/\sqrt{\eta\tau_Q}$ in (a). $\tilde{\varphi} = \tau_Q^{1/3}\varphi$, $\tilde{t} = t/\tau_Q^{1/3}$ in (b). $\varphi(0) = 10^{-4}$ and various quench timescales τ_Q . The dashed line represents $\tilde{\varphi} = \sqrt{\epsilon(\tilde{t})}$, the location of the broken symmetry minimum of the potential V .

Therefore, the freezeout time \hat{t} obeys the relationship [3, 16]:

$$\hat{t} \propto \tau_Q^{1/3} \quad (10)$$

in the underdamped case.

Equation (1) that dictates the evolution of the order parameter and is used to study formation of topological defects can have, in general, both first- and second-order time-derivative terms. As we have seen, purely overdamped and purely underdamped temporal evolution leads to different scaling of \hat{t} and of the defect density. The question then arises: What is the scaling when both $\dot{\varphi}$ and φ are present?

Evolution generated by Eq. (1) is—in the spirit of the KZM—expected to be overdamped when $\eta\dot{\varphi} > \ddot{\varphi}$ at the freeze-out time \hat{t} . In this regime, the relaxation time $\tau_{\dot{\varphi}} \simeq |\varphi/\dot{\varphi}|$ scales with ϵ as: $\tau_{\dot{\varphi}} \simeq \eta|\epsilon|^{-1} \simeq \eta\tau_Q|t|^{-1}$. In accord with [3], one expects the size $\hat{\xi}$ of the domains of the new broken symmetry phase to be set at the time \hat{t} , when the time to (from) the phase transition is comparable to the relaxation timescale, and the freeze-out of the field configuration occurs as a result of critical slowing down.

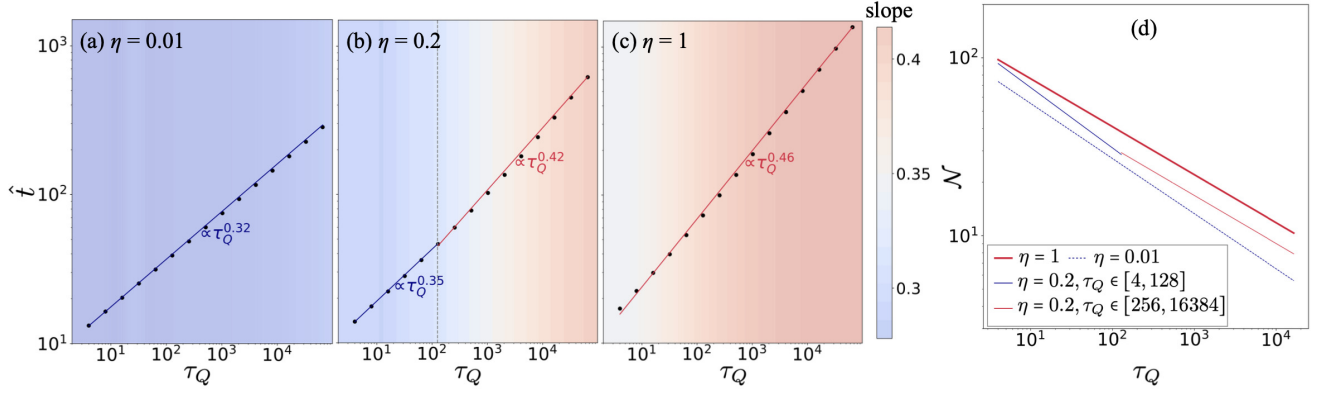


FIG. 6: Transition of the freeze-out time scaling between the underdamped and overdamped regimes, obtained from the location of the inflection point of the solution to Eq. (2). The freeze-out time \hat{t} inferred from the first inflection point where $\ddot{\varphi} = 0$ as a function of the quench timescale τ_Q for damping constants (a) $\eta = 0.01$, (b) $\eta = 0.2$, and (c) $\eta = 1$, with $\varphi(0) = 10^{-4}$. The color plot represents the slope of the log plot based on nearest neighbor points. For $\eta = 0.2$, a transition from the underdamped regime to the overdamped regime is observed as τ_Q increases. The dashed gray line represents the theoretical prediction $\tau_Q = 1/\eta^3$ where the transition from underdamped to overdamped scaling occurs [16]. (d) The number of defects \mathcal{N} as the function of τ_Q for $\eta = 0.01$ (dashed blue line), $\eta = 0.2$ (solid blue line for $\tau_Q \in [4, 128]$ and solid red line for $\tau_Q \in [128, 16384]$), and $\eta = 1$ (thick red line) with $\theta = 10^{-8}$. \mathcal{N} is obtained by numerically solving the full Langevin PDE (Eq. (1)) in (1+1) dimensions for a real scalar field.

This freeze-out condition, $\tau_{\dot{\varphi}}(\hat{t}_{\dot{\varphi}}) = \hat{t}_{\dot{\varphi}}$ yields in this case;

$$\hat{t}_{\dot{\varphi}} \simeq (\eta \tau_Q)^{1/2}, \quad \hat{\epsilon}_{\dot{\varphi}} \simeq \left(\frac{\eta}{\tau_Q} \right)^{1/2}. \quad (11)$$

The correlation length $\hat{\xi}$ which sets the stage for the defect formation is then:

$$\hat{\xi}_{\dot{\varphi}} \simeq \frac{\xi_o}{|\hat{\epsilon}_{\dot{\varphi}}|^{1/2}} \simeq \xi_o \left(\frac{\tau_Q}{\eta} \right)^{1/4}. \quad (12)$$

The density of the number of kinks is given by

$$\mathcal{N}_{\dot{\varphi}} \simeq \frac{1}{\hat{\xi}_{\dot{\varphi}}} \propto \left(\frac{\eta}{\tau_Q} \right)^{1/4}. \quad (13)$$

In the underdamped case, $\ddot{\varphi}$ will dominate, and the order parameter reacts to the quench-induced changes in the effective potential on the timescale $\tau_{\ddot{\varphi}} \simeq |\varphi/\ddot{\varphi}|^{1/2}$. Thus, $\tau_{\ddot{\varphi}} \simeq \tau_o |\epsilon|^{-1/2}$. The freeze-out condition, $\tau_{\ddot{\varphi}}(\hat{t}_{\ddot{\varphi}}) = \hat{t}_{\ddot{\varphi}}$ yields in this underdamped regime:

$$\hat{t}_{\ddot{\varphi}} \simeq (\tau_Q/\tau_o)^{1/3}, \quad \hat{\epsilon}_{\ddot{\varphi}} \simeq (\tau_o/\tau_Q)^{2/3}. \quad (14)$$

Consequently, the scaling of the characteristic correlation length with the quench time τ_Q is expected to change to

$$\hat{\xi}_{\ddot{\varphi}} \simeq \frac{\xi_o}{|\hat{\epsilon}_{\ddot{\varphi}}|^{1/2}} \simeq \xi_o \tau_Q^{1/3}. \quad (15)$$

Furthermore, the density of the number of kinks is given in this case by:

$$\mathcal{N}_{\ddot{\varphi}} \simeq \frac{1}{\hat{\xi}_{\ddot{\varphi}}} \propto \left(\frac{1}{\tau_Q} \right)^{1/3}. \quad (16)$$

We can therefore draw two related conclusions: (i) In the overdamped regime, the density of kinks should scale with $\eta^{1/4}$, and should become viscosity independent in the underdamped case. (ii) Power-law dependence of the density of kinks with the quench timescale should change from $\propto \tau_Q^{-1/4}$ in the overdamped case to $\propto \tau_Q^{-1/3}$ in the underdamped case. The overdamped scalings should apply when the evolution is dominated by the first derivative ($\eta \dot{\varphi} > \ddot{\varphi}$, i.e., $\eta/\tau_{\dot{\varphi}} > 1/\tau_{\ddot{\varphi}}^2$) at the instant when topological defects freeze-out. This will happen for: $|\hat{\epsilon}_{\dot{\varphi}}| > |\hat{\epsilon}_{\ddot{\varphi}}|$, or—using Eq. (11) and (14)—when:

$$\eta^3 > 1/\tau_Q,$$

as discussed in [16].

We have seen that the freeze-out time \hat{t} can be determined directly from the location of the inflection point of the solution of Eq. (2). Analyzing the solution of the ODE without assuming either the overdamped or underdamped limits reveals the transition from the scaling behavior of the overdamped regime to that of the underdamped regime. We rely on the observation that the freeze-out time $+\hat{t}$ is the moment when the solution $\varphi(t)$ begins to move rapidly toward the broken symmetry potential minima after $t = 0$. This happens at the inflection point when the second time-derivative $\ddot{\varphi} = 0$ for the first time after $t = 0$. In Fig. 6, \hat{t} identified as such inflection point is plotted as a function of the quench timescale τ_Q for (a) $\eta = 0.01$, (b) $\eta = 0.2$, and (c) $\eta = 1$, with $\varphi(0) = 10^{-4}$.

In Fig. 6 (a-c), the color plots reflect the slope of the log plot based on nearest neighbor points. It is found that $\hat{t} \propto \tau_Q^{0.46}$ for $\eta = 1$ and $\hat{t} \propto \tau_Q^{0.32}$ for $\eta = 0.01$; Both closely

align with the relations given by Eqs. (9,10) respectively, as predicted in [16]. The color plot reveals a transition from the underdamped regime to the overdamped regime as τ_Q increases for $\eta = 0.2$. We have that $\hat{t} \propto \tau_Q^{0.35}$ for $\tau_Q \in [4, 128]$ and $\hat{t} \propto \tau_Q^{0.42}$ for $\tau_Q \in [128, 16384]$. The gray dashed line represents the theoretical prediction, $\tau_Q = 1/\eta^3$, where the gradual transition between the overdamped ($\hat{t} \sim \tau_Q^{\frac{1}{2}}$) and underdamped ($\hat{t} \sim \tau_Q^{\frac{1}{3}}$) regime is expected [16].

Fig. 6 (d) shows the number of defects \mathcal{N} created by phase transitions as a function of τ_Q . This result is obtained by numerically solving the full PDE (Eq. (1)) in (1+1) dimensions with $\theta = 10^{-8}$ (Appendix). In the underdamped case with $\eta = 0.01$, the number of defects $\mathcal{N} \propto \tau_Q^{-0.31}$ (dashed blue line), while $\mathcal{N} \propto \tau_Q^{-0.27}$ in the overdamped case with $\eta = 1$ (thick red line). For $\eta = 0.2$, we observe a change in the scaling of the number of defects. We have $\mathcal{N} \propto \tau_Q^{-0.34}$ for small quench timescales $\tau_Q \in [4, 128]$ and $\mathcal{N} \propto \tau_Q^{-0.27}$ for large quench timescales $\tau_Q \in [128, 16384]$. The scaling of the number of defects ($\mathcal{N} \sim \tau_Q^{-\frac{1}{3}}$ to $\mathcal{N} \sim \tau_Q^{-\frac{1}{4}}$) corresponds to the change in the scaling of the freeze-out time \hat{t} from the underdamped to the overdamped regime as τ_Q increases. This is anticipated by the KZM based on the analysis of the consequences of critical slowing down [3, 16], but it can be predicted solely by solving simple ODE (Eq. (2)).

FREEZE-OUT OF THE SPATIAL STRUCTURE AT \hat{t}

We now turn to the question: How is the timescale \hat{t} imprinted on the spatial structure of $\Phi(x, t)$? To address this, we consider the equation obtained by removing the time dependence and the noise term from Eq. (1). The resulting equation for the spatial dependence of $\Phi(x, t)$ is:

$$\nabla^2 \phi(\mathbf{x}) - \partial_\phi V(\phi) = 0. \quad (17)$$

It is solved by

$$\phi(x) = \phi(0) \text{cd} \left(\frac{i\sqrt{\phi(0)^2 - 2\epsilon}x}{2}, -\frac{\phi(0)^2}{\phi(0)^2 - 2\epsilon} \right) \quad (18)$$

in 1-dimensional case where $\phi(0) = \phi(x=0)$, $\phi'(0) = 0$ and cd represents Jacobi elliptic function. Eq. (18) can be approximated by $\phi(x) = \phi(0) \cos \sqrt{\epsilon/2}x$ for small $|\phi(0)| \ll \sqrt{\epsilon}$ when $\epsilon > 0$. It exhibits spatial periodicities related to $1/\sqrt{\epsilon}$. Of particular interest is the periodicity $1/\sqrt{\hat{\epsilon}}$ that emerges for small ϕ near $\pm \hat{t}$ when the order parameter $\Phi(x, t)$ begins to grow from the small fluctuations bestowed during the $[-\hat{t}, +\hat{t}]$ interval by the random walk $\vartheta(x, t)$ in the Langevin equation Eq. (1), and rises to the broken symmetry equilibrium $\sqrt{\epsilon}$. Focusing on its

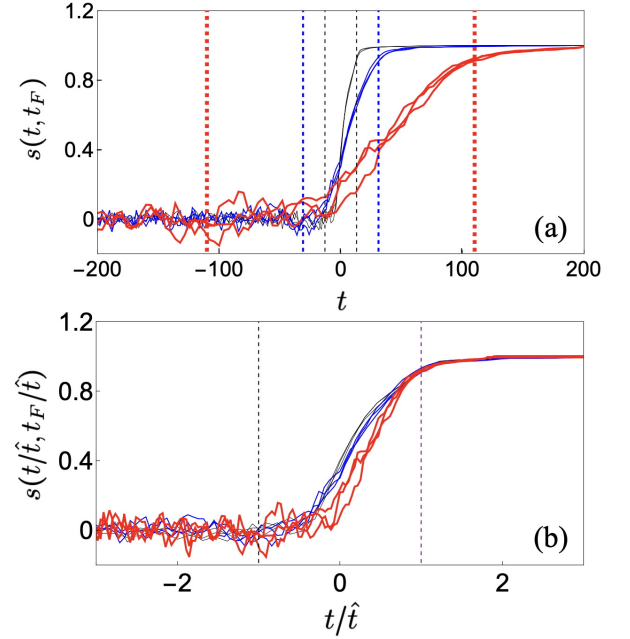


FIG. 7: Gradual evolution of $\Phi(x, t)$ toward its final configuration, obtained by numerically solving the full Langevin PDE (Eq. (1)) in (1+1) dimensions for a real scalar field. The time-correlation function $s(t, t_F)$ (Eq. (20)) for $\theta = 10^{-2}$, and three symmetry-breaking evolutions for each of three quench times: $\tau_Q = 8$ (thin, black), $\tau_Q = 64$ (blue), and $\tau_Q = 512$ (thick, red). The locations of topological defects settle by $t_F = 200$, and the correlation function approaches the asymptotic value of 1 when $\Phi(x, t)$ and $\Phi(x, t_F)$ are obtained from the same run—otherwise $s(t, t_F) \approx 0$. The correlation function $s(t, t_F)$ in (a) is plotted as the function of t . The vertical dashed lines indicate $\pm \hat{t}$ for each τ_Q , while (b) $s(t, t_F)$ is plotted as a function of rescaled time t/\hat{t} , where the purple line indicates $\pm \hat{t}$ for this case. Now the plots for different τ_Q nearly overlap, confirming the universality predicted by the KZM.

spatial part, we can think of the local $\phi(x)$ as a consequence of the random walk filtered by the spatial component of the Langevin equation, Eq. (17). That filtering attempts to impose periodicities (set by the “spring constant” $\sim \hat{\epsilon}$) of the Jacobi function (which represents the solution of the “physical pendulum”). That spatial period is exactly $\sim 1/\sqrt{\hat{\epsilon}}$, as for small values of ϕ the effect of the nonlinearity in Eq. (17) can be neglected. This yields

$$\hat{\epsilon} \sim \begin{cases} (\tau_Q/\eta)^{1/4}, & \text{(overdamped case)} \\ \tau_Q^{1/3}, & \text{(underdamped case)} \end{cases} \quad (19)$$

This structure is both imprinted and erased on $\Phi(x, t)$ by the combination of the filtering and random walk due to the noise term in the interval $[-\hat{t}, +\hat{t}]$. It firms up only after $\pm \hat{t}$, as the order parameter settles into the potential minima associated with broken symmetry.

The evidence of its gradual accumulation, which for $t > +\hat{t}$ leads to the formation of well-defined topological defects, can be seen in the time-correlation function (Eq. (20)) with the final configuration $\Phi(x, t_F)$, evaluated at t_F , the time after the system has settled to its post-transition state following $+\hat{t}$. It is a measure of the proximity of evolving $\Phi(x, t)$ with the final configuration:

$$s(t, t_F) = \frac{\sum_x \Phi(x, t) \Phi(x, t_F)}{\sqrt{\sum_x \Phi(x, t)^2} \sqrt{\sum_x \Phi(x, t_F)^2}}. \quad (20)$$

In Fig. 7 (a), we see that $s(t, t_F)$ begins to rise already somewhat before the critical point is traversed, but after $-\hat{t}$, and reaches its equilibrium value shortly after $+\hat{t}$ when, according to [3], the basic structure of the broken symmetry state (including the location of the defects) is determined. This confirms the adiabatic-impulse-adiabatic parsing of the dynamics of symmetry breaking quenches. Furthermore, panel (b) presents $s(t, t_F)$ as a function of the rescaled time t/\hat{t} , demonstrating that the curves for different τ_Q closely overlap, in agreement with the universality predicted by the KZM.

We note that, while our discussion was focused on the Langevin equation for Landau-Ginzburg and Gross-Pitaevskii models of the phase transition in 1+1 dimension, periodicities related to the solutions of Eq. (17) will arise as long as the Laplacian operator ∇^2 is involved, regardless of the number of spatial dimensions. This appears to be the case in systems where the sonic horizon motivation for the KZM is difficult to invoke, as the propagation of the front of the broken symmetry involves diffusion rather than sound, or is a subject to other constraints (e.g., involves a conserved order parameter).

DISCUSSION

The KZM predicts consequences of nonequilibrium phase transitions in diverse settings including condensed matter [10, 11, 21, 22, 28, 30–57], chemistry [58, 59], quantum computing [14, 60–76], cosmology [1–5, 77–81], and in other systems where a spatially uniform pretransition state is forced to undergo symmetry breaking. While creation of topological defects and other excitations in nonequilibrium phase transitions is the best known application, the KZM has been successfully used to study structure formation in transitions between steady states in systems such as Rayleigh-Benard instability [13].

The cornerstone of the KZM is the conjecture that the size of the domains that choose the same broken symmetry corresponds to the equilibrium correlation (or healing) length at the instant when the relaxation rate of the system equals to the speed with which the relevant (e.g., thermodynamic) potential is changing [3]. This leads to the KZM scaling that predicts the dependence of the size of domains in the post-transition state on the quench rate. It is by now widely tested in both laboratory and numerical experiments and verified whenever the assumptions that lead to the KZM hold.

The question we considered is why the KZM works so well. To address it we examined a paradigmatic model—a field theory with the time-dependent Landau-Ginzburg potential—where the KZM is known to hold, as the density of topological defects (e.g., “kinks”) generated by quench follows the KZM scaling [15, 16]. To understand why the KZM works so well we deconstructed the PDE used to study the KZM and examined the role of its components, starting with the ODE responsible for temporal evolution.

The advantage of this “piecewise” approach is evident: Temporal ODE is easy to integrate. Moreover, in the overdamped case it reduces to the analytically solvable Bernoulli equation. The time-dependent evolution of the order parameter exhibits features—e.g., marks the instants $\pm\hat{t}$ —that have been identified (on the basis of heuristic arguments) as the cornerstones of the scaling predictions of the KZM. These two instants mark the end and the beginning of the time intervals where the order parameter can adiabatically follow the potential imposed externally. Between these two instants—in the time interval delineated by $-\hat{t}$ and $+\hat{t}$ —the reaction time of order parameter of the system is too slow to allow for adiabatic evolution. In the pre-transition period that ends at the critical point at $t = 0$ the order parameter is buffeted by noise. It is especially vulnerable to the noise after $t = -\hat{t}$ is traversed, as the restoring force of the quadratic part of the potential is too weak to reimpose the pre-transition symmetric equilibrium state. Thus, after the critical point is traversed, the instability at $t > 0$ begins to dominate the evolution as the order parameter starts with a small but non-negligible initial (i.e., at $t \approx 0$) value imposed by the noise-driven random walk.

The subsequent evolution in the “upside down” harmonic oscillator potential amplifies the $\Phi(x, t = 0)$ configuration. The order parameter that was “primed” by fluctuations will start to evolve towards one of the broken symmetry minima. The expected values of $\Phi(x, t = 0)$ are easy to estimate but are difficult to calculate precisely, as the spatial part plays the role. Fortunately, their effect on \hat{t} —the crucial element of the KZM—is only logarithmic (hence, negligible).

This rapid (superexponential) evolution for $t > 0$ slows down only at $t \gtrsim +\hat{t}$, as the local broken symmetry minimum is reached. The structure of the post-transition configuration of the order parameter—including, in particular, topological defects—is then seeded by the fluctuations. Topology stabilizes defects after $+\hat{t}$, although annihilation is still possible. Their density is largely determined by the size of the broken-symmetry domains at $+\hat{t}$.

Spatial part of Eq. (1) plays a key supporting role, as it exhibits spatial periodicity related to \hat{t} which, at freeze-out time, corresponds to $\hat{\xi}$. Thus, fluctuations pass through the filter that favors structures with the approximate spatial periodicity of $\hat{\xi}$. This reasoning applies whenever the homotopy group allows for existence of topological defects [1], and whenever the spatial part

of the evolution includes the Laplacian operator. When the order parameter is complex, phase ordering can be rapid, but in a closed loop—at least in the 1D case we investigated—it will leave winding numbers with the expectation values that can be estimated from the quench rate [3]. The scaling of the expected winding numbers depends on the rate of the transition and the size of the loop: When the diameter of the loop is large compared to ξ , the winding number will be given by the square root of the number of defects that are expected to form inside that loop. When the loop has diameter comparable or smaller than ξ , the probability of trapping a winding number is given by the probability of finding a single defect within the loop of that size [82].

Previous studies of the KZM have primarily focused on testing the power-law scaling it predicts. This work highlights the role of the dynamics of the order parameter, which should be directly accessible in experiments, and could provide important insight into the foundational conjecture underlying the KZM. The time evolution of the order parameter, such as magnetization, polarization, or BEC density, is often an experimentally observable quantity. Remarkably, as demonstrated in this paper, these dynamics of the order parameters can be described by simple, often exactly solvable ODEs. Symmetry breaking dynamics in second order phase transi-

tions has been so far studied indirectly, primarily through the quench rate dependence of the density of topological defects—relics of such phase transitions. Our results suggest a possibility of a more direct approach—following the evolution of the order parameter. This is in a sense an approach complementary, yet (as we have seen) closely tied to the emergence of defects. It is certainly possible to monitor growth of the order parameter (see, for example, analysis of the time-dependent growth of the condensate density in [83], and experimental results such as [84–86]). It remains to be seen whether dedicated experiments can be done with sufficient temporal resolution and in systems that are uniform enough so that the spurious spatial gradients do not obscure the growth of the order parameter predicted by the relevant ODE. In addition to these implications for potential future tests, the study of order-parameter dynamics presented in this paper has recently inspired the use of machine learning to predict the locations of topological defects [87].

ACKNOWLEDGMENTS

We thank John Bowlan for helpful discussions. F.S. acknowledges support from the Los Alamos National Laboratory LDRD program under project number 20230049DR and the Center for Nonlinear Studies under project number 20250614CR-NLS.

-
- [1] T. W. B. Kibble. Topology of cosmic domains and strings. *Journal of Physics A: Mathematical and General*, 9(8):1387, aug 1976.
 - [2] T.W.B. Kibble. Some implications of a cosmological phase transition. *Physics Reports*, 67(1):183–199, 1980.
 - [3] W. H. Zurek. Cosmological experiments in superfluid helium? *Nature*, 317(6037):505–508, 1985.
 - [4] W. H. Zurek. Cosmic strings in laboratory superfluids and the topological remnants of other phase transitions. *Acta Phys. Polon. B*, 24:1301–1311, 1993.
 - [5] W. H. Zurek. Cosmological experiments in condensed matter systems. *Physics Reports*, 276(4):177–221, 1996.
 - [6] Adolfo del Campo and Wojciech H. Zurek. Universality of phase transition dynamics: Topological defects from symmetry breaking. *International Journal of Modern Physics A*, 29(08):1430018, 2014.
 - [7] Debasis Sadhukhan, Aritra Sinha, Anna Francuz, Justyna Stefaniak, Marek M Rams, Jacek Dziarmaga, and Wojciech H Zurek. Sonic horizons and causality in phase transition dynamics. *Physical Review B*, 101(14):144429, 2020.
 - [8] Bogdan Damski and Wojciech H Zurek. Dynamics of a quantum phase transition in a ferromagnetic bose-einstein condensate. *Physical review letters*, 99(13):130402, 2007.
 - [9] Austen Lamacraft. Quantum quenches in a spinor condensate. *Physical review letters*, 98(16):160404, 2007.
 - [10] Sven Deutschländer, Patrick Dillmann, Georg Maret, and Peter Keim. Kibble-Zurek mechanism in colloidal monolayers. *Proceedings of the National Academy of Sciences*, 112(22):6925–6930, 2015.
 - [11] Shi-Zeng Lin, Xueyun Wang, Yoshitomo Kamiya, Gia-Wei Chern, Fei Fan, David Fan, Brian Casas, Yue Liu, Valery Kiryukhin, Wojciech H Zurek, et al. Topological defects as relics of emergent continuous symmetry and Higgs condensation of disorder in ferroelectrics. *Nature Physics*, 10(12):970–977, 2014.
 - [12] S Ducci, Pier Luigi Ramazza, Wenceslao González-Viñas, and FT Arecchi. Order parameter fragmentation after a symmetry-breaking transition. *Physical Review Letters*, 83(25):5210, 1999.
 - [13] S Casado, Wenceslao González-Viñas, and H Mancini. Testing the kibble-zurek mechanism in rayleigh-bénard convection. *Physical Review E—Statistical, Nonlinear, and Soft Matter Physics*, 74(4):047101, 2006.
 - [14] Bogdan Damski. The simplest quantum model supporting the Kibble-Zurek mechanism of topological defect production: Landau-Zener transitions from a new perspective. *Physical review letters*, 95(3):035701, 2005.
 - [15] Pablo Laguna and Wojciech H Zurek. Density of kinks after a quench: When symmetry breaks, how big are the pieces? *Phys. Rev. Lett.*, 78:2519–2522, Mar 1997.
 - [16] Pablo Laguna and Wojciech H Zurek. Critical dynamics of symmetry breaking: Quenches, dissipation, and cosmology. *Physical Review D*, 58(8):085021, 1998.
 - [17] Andrew Yates and Wojciech H Zurek. Vortex formation in two dimensions: When symmetry breaks, how big are the pieces? *Physical review letters*, 80(25):5477, 1998.

- [18] Nuno D Antunes, Luis MA Bettencourt, and Wojciech H Zurek. Vortex string formation in a 3D U (1) temperature quench. *Physical review letters*, 82(14):2824, 1999.
- [19] Jacek Dziarmaga, Pablo Laguna, and Wojciech H Zurek. Symmetry breaking with a slant: topological defects after an inhomogeneous quench. *Physical review letters*, 82(24):4749, 1999.
- [20] Fumika Suzuki and Wojciech H Zurek. Topological defect formation in a phase transition with tunable order. *Physical Review Letters*, 132(24):241601, 2024.
- [21] Bogdan Damski and Wojciech H Zurek. Soliton creation during a Bose-Einstein condensation. *Physical review letters*, 104(16):160404, 2010.
- [22] Jacopo Sabbatini, Wojciech H Zurek, and Matthew J Davis. Phase separation and pattern formation in a binary Bose-Einstein condensate. *Physical review letters*, 107(23):230402, 2011.
- [23] Mithun Thudiyangal and Adolfo del Campo. Universal vortex statistics and stochastic geometry of Bose-Einstein condensation. *Physical Review Research*, 6(3):033152, 2024.
- [24] SP Cockburn and NP Proukakis. The stochastic Gross-Pitaevskii equation and some applications. *Laser Physics*, 19:558–570, 2009.
- [25] RG McDonald and AS Bradley. Reservoir interactions during Bose-Einstein condensation: Modified critical scaling in the Kibble-Zurek mechanism of defect formation. *Physical Review A*, 92(3):033616, 2015.
- [26] Arnab Das, Jacopo Sabbatini, and Wojciech H Zurek. Winding up superfluid in a torus via Bose Einstein condensation. *Scientific reports*, 2(1):352, 2012.
- [27] P Blair Blakie, AS Bradley, MJ Davis, RJ Ballagh, and CW Gardiner. Dynamics and statistical mechanics of ultra-cold bose gases using c-field techniques. *Advances in Physics*, 57(5):363–455, 2008.
- [28] Julian Sonner, Adolfo Del Campo, and Wojciech H Zurek. Universal far-from-equilibrium dynamics of a holographic superconductor. *Nature communications*, 6(1):7406, 2015.
- [29] Noble Gluscevich and JA Sauls. Kibble-zurek dynamics and statistics of topological defects in chiral superfluid he 3 films. *Physical Review B*, 111(21):214526, 2025.
- [30] A Maniv, E Polturak, and G Koren. Observation of magnetic flux generated spontaneously during a rapid quench of superconducting films. *Physical review letters*, 91(19):197001, 2003.
- [31] Wojciech H Zurek and Uwe Dörner. Phase transition in space: how far does a symmetry bend before it breaks? *Philosophical Transactions of the Royal Society A: Mathematical, Physical and Engineering Sciences*, 366(1877):2953–2972, 2008.
- [32] Charles Reichhardt and C. J. O. Reichhardt. Melting, reentrant ordering and peak effect for Wigner crystals with quenched and thermal disorder. *New Journal of Physics*, 25(4):043016, 2023.
- [33] C. Reichhardt and C. J. O. Reichhardt. Kibble-zurek scenario and coarsening across nonequilibrium phase transitions in driven vortices and skyrmions. *Phys. Rev. Res.*, 5:033221, Sep 2023.
- [34] Michael Uhlmann, Ralf Schützhold, and Uwe R Fischer. Vortex quantum creation and winding number scaling in a quenched spinor bose gas. *Physical review letters*, 99(12):120407, 2007.
- [35] Aritra Sinha, Marek M Rams, and Jacek Dziarmaga. Kibble-zurek mechanism with a single particle: Dynamics of the localization-delocalization transition in the Aubry-André model. *Physical Review B*, 99(9):094203, 2019.
- [36] Jacek Dziarmaga and Jakub M Mazur. Tensor network simulation of the quantum Kibble-Zurek quench from the Mott to the superfluid phase in the two-dimensional Bose-Hubbard model. *Physical Review B*, 107(14):144510, 2023.
- [37] Mithun Thudiyangal and Adolfo del Campo. Universal vortex statistics and stochastic geometry of bose-einstein condensation. *Physical Review Research*, 6(3):033152, 2024.
- [38] Francis A Bayocboc Jr, Jacek Dziarmaga, and Wojciech H Zurek. Biased dynamics of the miscible-immiscible quantum phase transition in a binary Bose-Einstein condensate. *Physical Review B*, 109(6):064501, 2024.
- [39] Emilia Witkowska, Piotr Deuar, Mariusz Gajda, and K Rzazewski. Solitons as the early stage of quasicondensate formation during evaporative cooling. *Physical Review Letters*, 106(13):135301, 2011.
- [40] Raz Carmi, Emil Polturak, and Gad Koren. Observation of spontaneous flux generation in a multi-Josephson-junction loop. *Physical review letters*, 84(21):4966, 2000.
- [41] R Monaco, Jesper Mygind, and RJ Rivers. Zurek-Kibble domain structures: The dynamics of spontaneous vortex formation in annular Josephson Tunnel junctions. *Physical review letters*, 89(8):080603, 2002.
- [42] LE Sadler, JM Higbie, SR Leslie, M Vengalattore, and DM Stamper-Kurn. Spontaneous symmetry breaking in a quenched ferromagnetic spinor Bose-Einstein condensate. *Nature*, 443(7109):312–315, 2006.
- [43] Chad N Weiler, Tyler W Neely, David R Scherer, Ashton S Bradley, Matthew J Davis, and Brian P Anderson. Spontaneous vortices in the formation of Bose-Einstein condensates. *Nature*, 455(7215):948–951, 2008.
- [44] Gabriele De Chiara, Adolfo Del Campo, Giovanna Morigi, Martin B Plenio, and Alex Retzker. Spontaneous nucleation of structural defects in inhomogeneous ion chains. *New Journal of Physics*, 12(11):115003, 2010.
- [45] Manuel Mielenz, J Brox, Steffen Kahra, Günther Leschhorn, Magnus Albert, Tobias Schätz, Haggai Landa, and Benni Reznik. Trapping of topological-structural defects in Coulomb crystals. *Physical review letters*, 110(13):133004, 2013.
- [46] S Ulm, J Roßnagel, G Jacob, C Degünther, ST Dawkins, UG Poschinger, R Nigmatullin, A Retzker, MB Plenio, F Schmidt-Kaler, et al. Observation of the kibble-zurek scaling law for defect formation in ion crystals. *Nature communications*, 4(1):2290, 2013.
- [47] K Pyka, J Keller, HL Partner, R Nigmatullin, T Burgermeister, DM Meier, K Kuhlmann, A Retzker, Martin B Plenio, WH Zurek, et al. Topological defect formation and spontaneous symmetry breaking in ion coulomb crystals. *Nature communications*, 4(1):2291, 2013.
- [48] SC Chae, N Lee, Y Horibe, M Tanimura, S Mori, B Gao, S Carr, and S-W Cheong. Direct observation of the proliferation of ferroelectric loop domains and vortex-antivortex pairs. *Physical review letters*, 108(16):167603, 2012.
- [49] Sinéad M Griffin, Martin Lilienblum, Kris T Delaney, Yu Kumagai, Manfred Fiebig, and Nicola A Spaldin. Scaling behavior and beyond equilibrium in the hexag-

- onal manganites. *Physical Review X*, 2(4):041022, 2012.
- [50] Simone Donadello, Simone Serafini, Marek Tylutki, Lev P Pitaevskii, Franco Dalfovo, Giacomo Lamporesi, and Gabriele Ferrari. Observation of solitonic vortices in Bose-Einstein condensates. *Physical review letters*, 113(6):065302, 2014.
- [51] Lauriane Chomaz, Laura Corman, Tom Bienaimé, Rémi Desbuquois, Christof Weitenberg, Sylvain Nascimbene, Jérôme Beugnon, and Jean Dalibard. Emergence of coherence via transverse condensation in a uniform quasi-two-dimensional bose gas. *Nature communications*, 6(1):6162, 2015.
- [52] Nir Navon, Alexander L Gaunt, Robert P Smith, and Zoran Hadzibabic. Critical dynamics of spontaneous symmetry breaking in a homogeneous Bose gas. *Science*, 347(6218):167–170, 2015.
- [53] J Rysti, JT Mäkinen, S Autti, T Kamppinen, GE Volovik, and VB Eltsov. Suppressing the Kibble-Zurek mechanism by a symmetry-violating bias. *Physical Review Letters*, 127(11):115702, 2021.
- [54] Hiroki Saito, Yuki Kawaguchi, and Masahito Ueda. Kibble-Zurek mechanism in a quenched ferromagnetic bose-einstein condensate. *Physical Review A—Atomic, Molecular, and Optical Physics*, 76(4):043613, 2007.
- [55] A. Libál, A. del Campo, C. Nisoli, C. Reichhardt, and C. J. O. Reichhardt. Quenched dynamics of artificial colloidal spin ice. *Phys. Rev. Res.*, 2:033433, Sep 2020.
- [56] CJO Reichhardt, A del Campo, and C Reichhardt. Kibble-Zurek mechanism for nonequilibrium phase transitions in driven systems with quenched disorder. *Communications physics*, 5(1):173, 2022.
- [57] Ian G Moss. Universal scaling law for quantum droplet formation. *arXiv preprint arXiv:2504.21641*, 2025.
- [58] Nikolai A Sinitsyn, Vijay Ganesh Sadhasivam, and Fumika Suzuki. Nonadiabatic transitions during a passage near a critical point. *The Journal of Chemical Physics*, 160(7), 2024.
- [59] Vijay Ganesh Sadhasivam, Fumika Suzuki, Bin Yan, and Nikolai A Sinitsyn. Parametric tuning of quantum phase transitions in ultracold reactions. *Nature Communications*, 15(1):10246, 2024.
- [60] Wojciech H Zurek, Uwe Dorner, and Peter Zoller. Dynamics of a quantum phase transition. *Physical review letters*, 95(10):105701, 2005.
- [61] Jacek Dziarmaga. Dynamics of a quantum phase transition: Exact solution of the quantum Ising model. *Physical review letters*, 95(24):245701, 2005.
- [62] Jacek Dziarmaga. Dynamics of a quantum phase transition and relaxation to a steady state. *Advances in Physics*, 59(6):1063–1189, 2010.
- [63] Anatoli Polkovnikov. Universal adiabatic dynamics in the vicinity of a quantum critical point. *Physical Review B—Condensed Matter and Materials Physics*, 72(16):161201, 2005.
- [64] Anatoli Polkovnikov, Krishnendu Sengupta, Alessandro Silva, and Mukund Vengalattore. Colloquium: Nonequilibrium dynamics of closed interacting quantum systems. *Reviews of Modern Physics*, 83(3):863–883, 2011.
- [65] Lukasz Cincio, Jacek Dziarmaga, Marek M Rams, and Wojciech H Zurek. Entropy of entanglement and correlations induced by a quench: Dynamics of a quantum phase transition in the quantum Ising model. *Physical Review A—Atomic, Molecular, and Optical Physics*, 75(5):052321, 2007.
- [66] Alexander Keesling, Ahmed Omran, Harry Levine, Hannes Bernien, Hannes Pichler, Soonwon Choi, Rhine Samajdar, Sylvain Schwartz, Pietro Silvi, Subir Sachdev, et al. Quantum kibble–zurek mechanism and critical dynamics on a programmable rydberg simulator. *Nature*, 568(7751):207–211, 2019.
- [67] Federico Balducci, András Grabarits, and Adolfo del Campo. Fighting exponentially small gaps by counterdiabatic driving. *arXiv preprint arXiv:2410.02520*, 2024.
- [68] Anne-Maria Visuri, Alejandro Gomez Cadavid, Balaganchi A Bhargava, Sebastián V Romero, András Grabarits, Pranav Chandarana, Enrique Solano, Adolfo del Campo, and Narendra N Hegade. Digitized counterdiabatic quantum critical dynamics. *arXiv preprint arXiv:2502.15100*, 2025.
- [69] Markus Schmitt, Marek M Rams, Jacek Dziarmaga, Markus Heyl, and Wojciech H Zurek. Quantum phase transition dynamics in the two-dimensional transverse-field Ising model. *Science Advances*, 8(37):eabl6850, 2022.
- [70] Andrew D King, Sei Suzuki, Jack Raymond, Alex Zucca, Trevor Lanting, Fabio Altomare, Andrew J Berkley, Sara Ejtemaee, Emile Hoskinson, Shuiyuan Huang, et al. Coherent quantum annealing in a programmable 2,000 qubit ising chain. *Nature Physics*, 18(11):1324–1328, 2022.
- [71] Andrew D King, Jack Raymond, Trevor Lanting, Richard Harris, Alex Zucca, Fabio Altomare, Andrew J Berkley, Kelly Boothby, Sara Ejtemaee, Colin Enderud, et al. Quantum critical dynamics in a 5,000-qubit programmable spin glass. *Nature*, 617(7959):61–66, 2023.
- [72] Yuki Bando, Yuki Susa, Hiroki Oshiyama, Naokazu Shibata, Masayuki Ohzeki, Fernando Javier Gómez-Ruiz, Daniel A Lidar, Sei Suzuki, Adolfo Del Campo, and Hidetoshi Nishimori. Probing the universality of topological defect formation in a quantum annealer: Kibble-zurek mechanism and beyond. *Physical Review Research*, 2(3):033369, 2020.
- [73] Bartłomiej Gardas, Jacek Dziarmaga, Wojciech H Zurek, and Michael Zwolak. Defects in quantum computers. *Scientific reports*, 8(1):4539, 2018.
- [74] Stefano Gherardini, Lorenzo Buffoni, and Nicolò Defenu. Universal defects statistics with strong long-range interactions. *Physical Review Letters*, 133(11):113401, 2024.
- [75] Phillip Weinberg, Marek Tylutki, Jami M Rönkkö, Jan Westerholm, Jan A Åström, Pekka Manninen, Päivi Törmä, and Anders W Sandvik. Scaling and diabatic effects in quantum annealing with a D-Wave device. *Physical Review Letters*, 124(9):090502, 2020.
- [76] Ralf Schützhold. Ultra-cold atoms as quantum simulators for relativistic phenomena. *Progress in Particle and Nuclear Physics*, page 104198, 2025.
- [77] Mark Hindmarsh, James A Sauls, Kuang Zhang, Samuli Autti, Richard P Haley, Petri J Heikkinen, Stephan J Huber, Lev V Levitin, Asier Lopez-Eiguren, Adam J Mayer, et al. Ab transition in superfluid ^3He and cosmological phase transitions. *Journal of Low Temperature Physics*, 215(5):495–524, 2024.
- [78] VMH Ruutu, VB Eltsov, AJ Gill, TWB Kibble, M Krusius, Yu G Makhlin, B Placais, GE Volovik, and Wen Xu. Vortex formation in neutron-irradiated superfluid ^3He as an analogue of cosmological defect formation. *Nature*, 382(6589):334–336, 1996.
- [79] Isaac Chuang, Ruth Durrer, Neil Turok, and Bernard Yurke. Cosmology in the laboratory: Defect dynamics in

- liquid crystals. *Science*, 251(4999):1336–1342, 1991.
- [80] C Bäuerle, Yu M Bunkov, SN Fisher, H Godfrin, and GR Pickett. Laboratory simulation of cosmic string formation in the early Universe using superfluid 3He. *Nature*, 382(6589):332–334, 1996.
- [81] Esteban A Calzetta and Bei-Lok B Hu. *Nonequilibrium quantum field theory*. Cambridge University Press, 2009.
- [82] Wojciech H Zurek. Topological relics of symmetry breaking: winding numbers and scaling tilts from random vortex–antivortex pairs. *Journal of Physics: Condensed Matter*, 25(40):404209, 2013.
- [83] I-K Liu, S Donadello, G Lamporesi, G Ferrari, S-C Gou, F Dalfovo, and NP Proukakis. Dynamical equilibration across a quenched phase transition in a trapped quantum gas. *Communications Physics*, 1(1):24, 2018.
- [84] H-J Miesner, DM Stamper-Kurn, MR Andrews, DS Durfee, S Inouye, and W Ketterle. Bosonic stimulation in the formation of a bose-einstein condensate. *Science*, 279(5353):1005–1007, 1998.
- [85] Mathilde Hugbart, Jocelyn A Retter, AF Varón, Philippe Bouyer, Alain Aspect, and Matthew J Davis. Population and phase coherence during the growth of an elongated bose-einstein condensate. *Physical Review A—Atomic, Molecular, and Optical Physics*, 75(1):011602, 2007.
- [86] Stephan Ritter, Anton Öttl, Tobias Donner, Thomas Bourdel, Michael Köhl, and Tilman Esslinger. Observing the formation of long-range order during bose-einstein condensation. *Physical review letters*, 98(9):090402, 2007.
- [87] Fumika Suzuki, Ying Wai Li, and Wojciech H Zurek. Machine learning topological defect formation. *arXiv preprint arXiv:2508.20347*, 2025.

NUMERICAL METHODS

We employed the 4th-order Runge-Kutta method to solve the full Langevin PDE (Eq. (1)) and the Gross-Pitaevskii equation (Eq. (5)) numerically. For the Langevin equation, we chose the system size $L = 2048$ with 4096 grid points. The number of defects \mathcal{N} shown in Fig. 6 (d) is obtained by numerically solving the full PDE (Eq. (1)) in (1+1) dimensions 15 times (i.e., 15 realizations of random noise), starting the time evolution at $\epsilon = -1$ and concluding it at $t = 32768$ (i.e., $\epsilon = 1$ for $\tau_Q = 16384$). For the stochastic Gross-Pitaevskii equation, we chose the system size $L = 30$ and 300 grid points to generate the plot in the Fig. 4.

CORRELATION LENGTH

In addition to the method used in the main text, we can also estimate the correlation length as follows. We consider the following equation that excludes the time dependence and the noise term from the Langevin equation Eq. (1) in the main text, and by introducing a delta-

function source $-\delta(x)$ at the origin:

$$\nabla^2 \phi(\mathbf{x}) - \partial_\phi V(\phi) = -\delta(\mathbf{x}). \quad (\text{S.1})$$

We assume $\phi(\mathbf{x}) = \phi_0(\mathbf{x}) + \delta\phi(\mathbf{x})$ where $\nabla^2 \phi_0(\mathbf{x}) - \partial_{\phi_0} V(\phi_0) = 0$ while the perturbation $\delta\phi$ obeys

$$\nabla^2 \delta\phi(\mathbf{x}) + \frac{1}{2}\epsilon(t)\delta\phi(\mathbf{x}) = -\delta(\mathbf{x}). \quad (\text{S.2})$$

Here the higher-order terms of $\delta\phi(\mathbf{x})$ are discarded. The solution of this equation takes the Ornstein-Zernike form:

$$\delta\phi(\mathbf{x}) \sim |\mathbf{x}|^{-(d-1)/2} \exp(-|\mathbf{x}|/\xi) \quad (\text{S.3})$$

in d -dimensional space and $\xi \sim 1/\sqrt{\epsilon}$. This yields

$$\hat{\xi} \sim \begin{cases} (\tau_Q/\eta)^{1/4}, & \text{(overdamped case)} \\ \tau_Q^{1/3}, & \text{(underdamped case)} \end{cases} \quad (\text{S.4})$$

where

$$\hat{t}_\phi \simeq (\eta \tau_Q)^{1/2}, \quad \hat{\epsilon}_\phi \simeq \left(\frac{\eta}{\tau_Q} \right)^{1/2} \quad (\text{S.5})$$

in the overdamped regime, and

$$\hat{t}_{\tilde{\phi}} \simeq (\tau_Q/\tau_o)^{1/3}, \quad \hat{\epsilon}_{\tilde{\phi}} \simeq (\tau_o/\tau_Q)^{2/3} \quad (\text{S.6})$$

in the underdamped regime from Eqs. (11, 14) in the main text.

GRADUAL CONVERGENCE OF DOMAIN SIZES TOWARDS $\hat{\xi}$

In addition to the correlation $s(t, t_F)$ with the final configuration shown in Fig. 7, we can also examine the evolution of the expected domain size to reveal the gradual accumulation of the order parameter. We identify the expected domain size with half of the spatial period, $\langle \lambda(t) \rangle$, obtained from the Fourier transform:

$$\frac{1}{\langle \lambda(t) \rangle} = \frac{1}{\mathcal{C}} \sum_k \frac{2k}{L} \tilde{\Phi}(k, t) \tilde{\Phi}^*(k, t) \quad (\text{S.7})$$

where $\tilde{\Phi}(k, t) = \sum_x \Phi(x, t) e^{-i2\pi kx/L}$, the normalization $\mathcal{C} = \sum_k \tilde{\Phi}(k, t) \tilde{\Phi}^*(k, t)$, and $L = 2048$ is the system size. Here, we consider half the spatial period $L/2k$ since the full period of the oscillation would produce a pair of kinks. Fig. 8 shows $\langle \lambda(t) \rangle$ as a function of τ_Q from $t = -\hat{t}$ to \hat{t} for the overdamped case with $\eta = 1$ (a) and for the underdamped case with $\eta = 0.01$ (b). The figure is obtained by averaging the results of 15 numerical simulations of Eq. (1). As time approaches \hat{t} , the behavior governed by the periodicity from the spatial component of the Langevin equation begins to dominate over that driven by the noise. The scaling of $\langle \lambda(t) \rangle$ eventually aligns closely with L/\mathcal{N} (i.e., the average domain size) at $t = \hat{t}$ where \mathcal{N} is the number of defects from Fig. 6 (d).

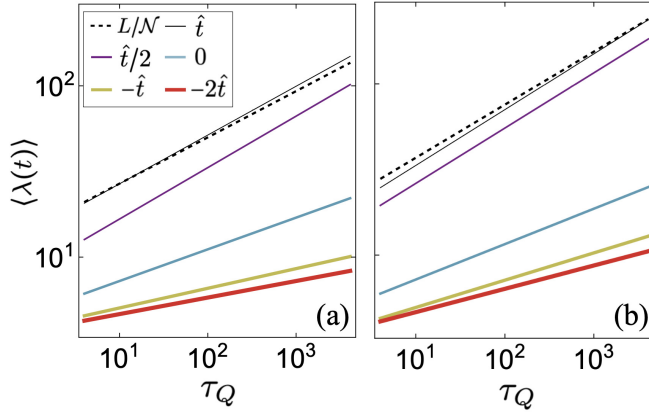


FIG. 8: **Gradual accumulation toward the final configuration of Φ .** $\langle \lambda(t) \rangle$ as a function of τ_Q for $\eta = 1$ (a) and for $\eta = 0.01$ (b). From thick red to thin black line, $t = -2\hat{t}, -\hat{t}, 0, \hat{t}/2, \hat{t}$ respectively. The dashed black lines represent L/\mathcal{N} (i.e., the average domain size) from Fig. 6 (d). $\theta = 10^{-8}$.